

DEGENERATE AREA PRESERVING SURFACE ALLEN–CAHN EQUATION AND ITS SHARP INTERFACE LIMIT

MICHAL BENEŠ, MIROSLAV KOLÁŘ, JAN MAGNUS SISCHKA, AND AXEL VOIGT*

Abstract. We consider formal matched asymptotics to show the convergence of a degenerate area preserving surface Allen–Cahn equation to its sharp interface limit of area preserving geodesic curvature flow. The degeneracy results from a surface de Gennes–Cahn–Hilliard energy and turns out to be essential to numerically resolve the dependency of the solution on geometric properties of the surface. We experimentally demonstrate convergence of the numerical algorithm, which considers a graph formulation, adaptive finite elements and a semi-implicit discretization in time, and uses numerical solutions of the sharp interface limit, also considered in a graph formulation, as benchmark solutions. The results provide the mathematical basis to explore the impact of curvature on cells and their collective behaviour. This is essential to understand the physical processes underlying morphogenesis.

Key words. Motion by geodesic curvature, surface Allen–Cahn equation, de Gennes–Cahn–Hilliard energy, matched asymptotic expansion, graph formulation.

1. Introduction

The connection between phase field approximations and geometric partial differential equations is well established and can formally be justified by matched asymptotics, see [1]. Geometric partial differential equations are evolution equations that evolve curves or surfaces according to their curvature. Prominent examples are mean curvature flow, area preserving mean curvature flow or surface diffusion, see [2, 3] for reviews. Similarly to these curvature driven flows in 2D or 3D one can consider the evolution of curves on surfaces. The evolution of these curves is governed by geodesic curvature and thus strongly depends on the local geometric properties of the underlying surface. First analytical attempts to connect these geodesic evolution laws to surface phase field models have been considered in [4, 5, 6, 7]. We here show this connection for a degenerate area preserving surface Allen–Cahn equation and an area preserving geodesic curvature flow.

This model is of particular interest in mathematical biology, where it is used to approximate cells in epithelial tissue [8, 9, 10]. These approaches are considered in 2D. Their extension to surfaces provides the mathematical basis to explore the impact of curvature on cells and their collective behaviour. This is essential to understand the physical processes underlying morphogenesis. First attempts in this direction [11, 12] show a huge impact of curvature on collective motion but also the sensitivity of the solution on local geometric properties of the surface, which asks for further mathematical foundations to which this paper contributes.

2. Mathematical models

We consider a surface de Gennes–Cahn–Hilliard energy

$$(1) \quad \mathcal{F}_{dGCH}(\phi) = \tilde{\sigma} \int_{\mathcal{S}} \frac{1}{G(\phi)} \left(\frac{\epsilon}{2} \|\nabla_S \phi\|^2 + \frac{1}{\epsilon} W(\phi) \right) d\mathcal{S}$$

Received by the editors on February 26, 2024 and, accepted on June 4, 2024.
2000 *Mathematics Subject Classification.* 35B36, 35K55, 35Q74.

*Corresponding author.

with surface \mathcal{S} , phase field variable ϕ , surface gradient $\nabla_{\mathcal{S}}$, double well potential $W(\phi) = \frac{1}{4}(\phi^2 - 1)^2$, rescaled surface tension $\tilde{\sigma}$ and small parameter $\epsilon > 0$ determining the thickness of the diffuse interface. The factor $1/G(\phi)$ is called the de Gennes coefficient in polymer science. We consider $G(\phi) = \frac{3}{2}(1 - \phi^2)$ or a regularized version $G_{\eta}(\phi) = (\frac{9}{4}(1 - \phi^2)^2 + \eta^2\epsilon^2)^{1/2}$ with $\eta > 0$. The scaling coefficient is such that the sharp interface limit equals the one obtained from the usual Cahn–Hilliard energy without the de Gennes coefficient [13, 14]. Evolution equations based on this energy, at least in 2D and 3D, have been shown numerically advantageous, as the singularity, $G(\phi)$ or $G_{\eta}(\phi)$, helps to keep solutions confined in $[-1, 1]$. However, a theoretical foundation of this argument remains open. From a practical point of view, the de Gennes coefficient allows to achieve the same accuracy with larger ϵ . Several numerical studies use this to achieve results which would not be possible without it, see [15, 16]. We will demonstrate that this advantage is also present on surfaces and becomes essential to numerically resolve the dependency of the solution on geometric properties of the surface.

The L^2 -gradient flow of eq. (1) on \mathcal{S} with an appropriate scaling in time reads

$$\begin{aligned} \epsilon\tilde{\beta}\partial_t\phi &= \tilde{\sigma} \left(\epsilon\nabla_{\mathcal{S}} \cdot \left(\frac{1}{G(\phi)} \nabla_{\mathcal{S}}\phi \right) - \frac{1}{\epsilon G(\phi)} W'(\phi) \right) \\ &\quad - \tilde{\sigma} \left(\frac{1}{G(\phi)} \right)' \left(\frac{\epsilon}{2} \|\nabla_{\mathcal{S}}\phi\|^2 + \frac{1}{\epsilon} W(\phi) \right), \end{aligned}$$

with surface divergence $\nabla_{\mathcal{S}} \cdot$ and Laplace–Beltrami operator $\Delta_{\mathcal{S}}$. $\tilde{\beta} > 0$ is a rescaled kinetic coefficient. Using the asymptotic approximation [17] $\frac{\epsilon}{2} \|\nabla_{\mathcal{S}}\phi\|^2 \approx \frac{1}{\epsilon} W(\phi)$ and the identity $\nabla_{\mathcal{S}} \cdot ((1/G(\phi))\nabla_{\mathcal{S}}\phi) = (1/G(\phi))\Delta_{\mathcal{S}}\phi + (1/G(\phi))' \|\nabla_{\mathcal{S}}\phi\|^2$ we can approximate this equation by

$$(2) \quad \epsilon\tilde{\beta}\partial_t\phi = \frac{\tilde{\sigma}}{G(\phi)} \left(\epsilon\Delta_{\mathcal{S}}\phi - \frac{1}{\epsilon} W'(\phi) \right).$$

The idea for this approximation was first used for phase field approximations of surface diffusion in [18], where $G(\phi)$ was introduced as a stabilizing function. Due to this approximation the gradient flow structure is lost. However, the computational cost is comparable to the formulation without $G(\phi)$. For a detailed derivation and numerical comparison of the full and the approximated formulation in 2D, see [13].

We now introduce the Lagrange multiplier λ in eq. (2) to ensure the area constraint $1/|\mathcal{S}| \int_{\mathcal{S}} \phi \, d\mathcal{S} = \alpha$ with $\alpha \in [-1, 1]$. The resulting system reads

$$(3) \quad \epsilon\tilde{\beta}\partial_t\phi = \frac{\tilde{\sigma}}{G(\phi)} \left(\epsilon\Delta_{\mathcal{S}}\phi - \frac{1}{\epsilon} W'(\phi) \right) + \lambda$$

$$(4) \quad \frac{1}{|\mathcal{S}|} \int_{\mathcal{S}} \phi \, d\mathcal{S} = \alpha.$$

By integrating eq. (3) over \mathcal{S} , and inserting the time derivative of eq. (4), we obtain

$$0 = \tilde{\sigma} \int_{\mathcal{S}} \frac{1}{G(\phi)} \left(\epsilon\Delta_{\mathcal{S}}\phi - \frac{1}{\epsilon} W'(\phi) \right) d\mathcal{S} + |\mathcal{S}|\lambda.$$

By solving for λ we arrive at the equation to be considered, a degenerate area preserving surface Allen–Cahn equation on \mathcal{S}

$$(5) \quad \epsilon\tilde{\beta}G(\phi)\partial_t\phi = \tilde{\sigma} \left(\epsilon\Delta_{\mathcal{S}}\phi - \frac{1}{\epsilon} W'(\phi) \right) + G(\phi)\lambda,$$

$$(6) \quad \lambda = \tilde{\sigma} \frac{1}{|\mathcal{S}|} \int_{\mathcal{S}} \left(-\frac{\epsilon}{G(\phi)} \Delta_{\mathcal{S}}\phi + \frac{1}{\epsilon G(\phi)} W'(\phi) \right) d\mathcal{S},$$

with initial condition $\phi(0) = \phi^0$. The zero-levelset of the solution of eqs. (5) and (6) provides an approximation of a closed curve γ evolving on the surface \mathcal{S} .

The area preserving geodesic curvature flow for the curve γ on \mathcal{S} reads

$$(7) \quad \beta \mathcal{V} = -\sigma \mathcal{H}_\gamma + \sigma \frac{1}{|\gamma|} \int_\gamma \mathcal{H}_\gamma \, d\gamma$$

with initial condition $\gamma(0) = \gamma^0$. \mathcal{V} is the velocity of $\gamma(t)$ in the direction of the co-normal μ and \mathcal{H}_γ is the geodesic curvature of γ . Let $\mathcal{S}^1 = \{(x, t) \in \mathcal{S} \times [0, T] : \phi(x, t) < 0\}$ and $\mathcal{S}^2 = \{(x, t) \in \mathcal{S} \times [0, t] : \phi(x, t) > 0\}$. Then $\mathcal{S} = \mathcal{S}^1(t) \cup \gamma(t) \cup \mathcal{S}^2(t)$ and we enforce the constraint $|\mathcal{S}^1(t)| - |\mathcal{S}^2(t)| + \alpha|\mathcal{S}| = 0$ for each $t \in [0, T]$. The kinetic coefficient and line tension are related by $\beta = 4\sqrt{2}/5\tilde{\beta}$ and $\sigma = 2\sqrt{2}/3\tilde{\sigma}$.

Besides the connection between eqs. (5) and (6) and eq. (7) by formal matched asymptotics, we use numerical solutions of eq. (7) in a graph formulation, see [19], as benchmark problems for a numerical approach to eqs. (5) and (6), again using a graph formulation. We use adaptive finite elements to discretize in space and a semi-implicit time-stepping scheme. While the asymptotic analysis also works out without the de Gennes coefficient $1/G(\phi)$, the numerical results demonstrate its necessity to achieve the required accuracy to resolve the dependency on geometric properties of the surface \mathcal{S} for reasonable values of ϵ .

3. Matched asymptotic analysis

We closely follow [7] in the analysis of a phase field model in the context of two-phase biomembranes and use the tools introduced in [4] to extend the formal matched asymptotics for the area preserving Allen–Cahn equations in flat space [20] and for the de Gennes–Cahn–Hilliard energy in flat space [13] to surfaces. We demonstrate that eqs. (5) and (6) formally converge to eq. (7) for $\epsilon \rightarrow 0$. We therefore require $\gamma(t)$ to be a C^2 closed curve.

3.1. Expansions and matching conditions. By $(\phi_\epsilon, \lambda_\epsilon)$, we denote a family of solutions of eqs. (5) and (6) that converge formally to some limit denoted by (ϕ, λ) . We assume that $\phi = \chi_\gamma$ with χ_γ a BV-function on \mathcal{S} with $\chi_\gamma = -1$ on \mathcal{S}^1 and $\chi_\gamma = 1$ on \mathcal{S}^2 for some smooth curve γ that separates the regions $\mathcal{S}^1 = \{(x, t) \in \mathcal{S} \times [0, T] : \phi(x, t) = -1\}$ and $\mathcal{S}^2 = \{(x, t) \in \mathcal{S} \times [0, t] : \phi(x, t) = 1\}$. We consider an outer and an inner expansion

$$(8) \quad f_\epsilon(x, t) = f_0(x, t) + \epsilon f_1(x, t) + \epsilon^2 f_2(x, t) + \dots$$

$$(9) \quad F_\epsilon(s, z, t) = F_0(s, z, t) + \epsilon F_1(s, z, t) + \epsilon^2 F_2(s, z, t) + \dots,$$

respectively, with $f_\epsilon(x, t) = F_\epsilon(s, z, t)$, $z = r/\epsilon$ and $\Theta(s, r, t)$ a parametrization such that $s \rightarrow \Theta(s, 0, t)$ is a parametrization of $\gamma(t)$ on \mathcal{S} and r is the signed geodesic distance of $x = \Theta(s, r, t) \in \mathcal{S}$ to $\partial\mathcal{S}^1$. We consider the outer and inner expansion of solutions $\phi_\epsilon, \lambda_\epsilon$ and write $f_\epsilon = \phi_\epsilon, \lambda_\epsilon$ and $F_\epsilon = \Phi_\epsilon, \Lambda_\epsilon$. The outer expansion holds away from $\gamma(t)$ and the inner expansion near $\gamma(t)$. In regions where both expansions are valid the following matching condition holds

$$(10) \quad F_0(s, \pm\infty, t) = f_0^\pm(x, t),$$

where we define $f_0^\pm(x, t) = \lim_{\delta \rightarrow 0} f_0(\Theta(s, \pm\delta, t), t)$ for a function $f_0(x, t) = f_0(\Theta(s, r, t), t)$.

3.2. Outer solution. Considering the terms of $O(\epsilon^{-1})$ in eq. (5) leads to $W'(\phi_0) = 0$ and thus the only stable solutions are

$$(11) \quad \phi_0 = \pm 1.$$

3.3. Inner solution. The Laplace–Beltrami operator and the total time derivative of $F_\epsilon(s, z, t)$ are

$$(12) \quad \Delta_{\mathcal{S}} F_\epsilon = \frac{1}{\epsilon^2} \partial_{zz} F_\epsilon + \frac{\mathcal{H}_\gamma}{\epsilon} \partial_z F_\epsilon + \partial_{ss} F_\epsilon + O(\epsilon)$$

$$(13) \quad \frac{d}{dt} F_\epsilon = -\frac{1}{\epsilon} \mathcal{V} \partial_z F_\epsilon + \partial_t F_\epsilon + O(\epsilon)$$

with ∂_{ss} the second derivative along γ . Considering terms of $O(\epsilon^{-1})$ in eq. (5) leads to $0 = \tilde{\sigma} (\partial_{zz} \Phi_0 - W'(\Phi_0))$. Using the outer expansion eq. (11) and the matching condition eq. (10) shows that $\Phi_0(s, z, t)$ is a solution of $\partial_{zz} \Phi_0 = W'(\Phi_0)$ with $\Phi_0(\pm\infty) = \pm 1$ and thus

$$(14) \quad \Phi_0(z) = \tanh\left(\frac{z}{\sqrt{2}}\right)$$

independent of s and t . Using this in $O(\epsilon^0)$ of eq. (5) leads to

$$(15) \quad -\tilde{\beta} \mathcal{V} G(\Phi_0) \partial_z \Phi_0 = \tilde{\sigma} (\mathcal{H}_\gamma \partial_z \Phi_0 - W''(\Phi_0) \Phi_1 + \partial_{zz} \Phi_1) + G(\Phi_0) \Lambda_0.$$

Multiplying by $\partial_z \Phi_0$ and integrating leads to

$$(16) \quad -\tilde{\beta} \mathcal{V} \int_{-\infty}^{+\infty} G(\Phi_0) (\partial_z \Phi_0)^2 dz = \tilde{\sigma} \int_{-\infty}^{+\infty} \mathcal{H}_\gamma (\partial_z \Phi_0)^2 - \partial_z W'(\Phi_0) \Phi_1 + \partial_{zz} \Phi_1 \partial_z \Phi_0 dz + \Lambda_0 \int_{-\infty}^{+\infty} G(\Phi_0) \partial_z \Phi_0 dz.$$

It holds

$$\int_{-\infty}^{+\infty} -\partial_z W'(\Phi_0) \Phi_1 + \partial_{zz} \Phi_1 \partial_z \Phi_0 dz = \int_{-\infty}^{+\infty} \Phi_1 \partial_z (-W'(\Phi_0) + \partial_{zz} \Phi_0) dz = 0$$

and thus

$$(17) \quad -\tilde{\beta} \mathcal{V} \int_{-\infty}^{+\infty} G(\Phi_0) (\partial_z \Phi_0)^2 dz = \tilde{\sigma} \mathcal{H}_\gamma \int_{-\infty}^{+\infty} (\partial_z \Phi_0)^2 dz + \Lambda_0 \int_{-\infty}^{+\infty} G(\Phi_0) \partial_z \Phi_0 dz.$$

With eq. (14) we obtain $\partial_z \Phi_0 = \frac{1}{\sqrt{2}} (1 - \Phi_0^2)$ and thus $\int_{-\infty}^{+\infty} G(\Phi_0) (\partial_z \Phi_0)^2 dz = \frac{4\sqrt{2}}{5}$, $\int_{-\infty}^{+\infty} (\partial_z \Phi_0)^2 dz = \frac{2\sqrt{2}}{3}$ and $\int_{-\infty}^{+\infty} G(\Phi_0) \partial_z \Phi_0 dz = 2$ and therefore

$$(18) \quad \beta \mathcal{V} = -\sigma \mathcal{H}_\gamma - 2\Lambda_0.$$

In order to determine Λ_0 we consider the constraint $\frac{1}{|\mathcal{S}|} \int_{\mathcal{S}} \phi_\epsilon d\mathcal{S} = \alpha$. Using eq. (13) in $O(\epsilon^{-1})$ gives $0 = \int_\gamma \mathcal{V} \partial_z \Phi_0 d\gamma$ and as $\partial_z \Phi_0$ is independent of s also $\int_\gamma \mathcal{V} d\gamma = 0$. Integrating eq. (18) we thus obtain

$$(19) \quad 2\Lambda_0 = -\sigma \frac{1}{|\gamma|} \int_\gamma \mathcal{H}_\gamma d\gamma$$

which leads to the desired eq. (7). This analysis is not affected by considering G_η instead of G and can also be done along the same lines without the de Gennes factor $1/G(\phi)$.

4. Graph formulations

Before we numerically solve both models, the degenerate area preserving surface Allen–Cahn equation (5) and (6) and the area preserving geodesic curvature flow (7), we reformulate them in a graph formulation. Assume that the surface \mathcal{S} is the graph of the function $h : \Omega \rightarrow \mathbb{R}$ where $\Omega \subseteq \mathbb{R}^2$ is a bounded domain, i.e.

$$\mathcal{S} = \{[\mathbf{x}, h(\mathbf{x})] \mid \mathbf{x} \in \Omega\}.$$

Let us also assume that the closed curve $\gamma(t) \subset \mathcal{S}$ is represented by a closed curve $g(t) \subset \Omega$, and the curve $g(t)$ is given by a 1-periodic parametrization $\mathbf{X} : (0, T) \times (0, 1) \rightarrow \Omega$ as $g(t) = \{\mathbf{X}(t, l) \mid t \in (0, T), l \in (0, 1)\}$, and consequently $\gamma(t) = \{[\mathbf{X}(t, l), h(\mathbf{X}(t, l))] \mid t \in (0, T), l \in (0, 1)\}$.

In [19] eq. (7) is transformed to the flow of $g(t)$

$$(20) \quad \beta V = -aH_g + b + c \frac{1}{\int_g \sqrt{1 + (\nabla h \cdot \mathbf{t}_g)^2} dg} \int_g \mathcal{H}_\gamma \sqrt{1 + (\nabla h \cdot \mathbf{t}_g)^2} dg$$

with the normal velocity V , the coefficients $a > 0$, b and c given as

$$a = \frac{\sigma}{1 + (\nabla h \cdot \mathbf{t}_g)^2}, \quad b = \frac{\sigma \mathbf{t}_g^T \nabla^2 h \mathbf{t}_g (\nabla h \cdot \mathbf{n}_g)}{(1 + (\nabla h \cdot \mathbf{t}_g)^2)(1 + |\nabla h|^2)}, \quad c = \sigma \sqrt{\frac{1 + (\nabla h \cdot \mathbf{t}_g)^2}{1 + |\nabla h|^2}}.$$

The unit tangent \mathbf{t}_g , unit outer normal \mathbf{n}_g and curvature H_g of the curve $g(t)$ are given as

$$(21) \quad \mathbf{t}_g = \frac{\partial_l \mathbf{X}}{|\partial_l \mathbf{X}|}, \quad \mathbf{n}_g = \frac{1}{|\partial_l \mathbf{X}|} (\partial_l X_2, -\partial_l X_1)^T, \quad H_g = -\frac{1}{|\partial_l \mathbf{X}|} \partial_l \left(\frac{\partial_l \mathbf{X}}{|\partial_l \mathbf{X}|} \right) \cdot \mathbf{n}_g$$

and the geodesic curvature \mathcal{H}_γ of $\gamma(t)$ is given as

$$(22) \quad \mathcal{H}_\gamma = -\frac{1}{\sqrt{1 + (\nabla h \cdot \mathbf{t}_g)^2}} \left(\sqrt{1 + |\nabla h|^2} H_g - \frac{\mathbf{t}_g^T \nabla^2 h \mathbf{t}_g}{\sqrt{1 + |\nabla h|^2}} (\nabla h \cdot \mathbf{n}_g) \right).$$

For details and the numerical realization we refer to [19, 21, 22].

The graph formulation for eq. (5) and (6) can be formulated as

$$(23) \quad \epsilon \tilde{\beta} G_\eta(\phi) \partial_t \phi = \tilde{\sigma} \psi - \frac{\tilde{\sigma} G_\eta(\phi)}{\int_\Omega \sqrt{1 + |\nabla h|^2} d\Omega} \int_\Omega \frac{\sqrt{1 + |\nabla h|^2}}{G_\eta(\phi)} \psi d\Omega$$

with $\psi = \epsilon \nabla \cdot \left(\left(I - \frac{(\nabla h)^2}{1 + |\nabla h|^2} \right) \nabla \phi \right) - \frac{1}{\epsilon} W'(\phi)$. As the Lagrange multiplier is evaluated explicitly numerical and truncation errors can accumulate over time, we follow [23] and introduce a relaxation rate for the Lagrange multiplier, which can also be interpreted as an additional penalization of the area of the form $\mu (1/|\mathcal{S}| \int_{\mathcal{S}} \phi d\mathcal{S} - \alpha)$, with penalization parameter μ . The resulting semi-discrete graph formulation with $\phi^n = \phi(t^n)$ reads

$$\begin{aligned} \epsilon \tilde{\beta} G_\eta(\phi^n) \frac{\phi^{n+1} - \phi^n}{\tau} &= \tilde{\sigma} \psi^{n+1} - \frac{\tilde{\sigma} G_\eta(\phi^n)}{\int_\Omega \sqrt{1 + |\nabla h|^2} d\Omega} \int_\Omega \frac{\sqrt{1 + |\nabla h|^2}}{G_\eta(\phi^n)} \psi^n d\Omega \\ &\quad - c \left(\frac{\int_\Omega \sqrt{1 + |\nabla h|^2} \phi^n d\Omega}{\int_\Omega \sqrt{1 + |\nabla h|^2} d\Omega} - \alpha \right), \end{aligned}$$

with $\psi^n = \epsilon \nabla \cdot \left(\left(I - \frac{(\nabla h)^2}{1 + |\nabla h|^2} \right) \nabla \phi^n \right) - \frac{1}{\epsilon} W'(\phi^n)$ and $W'(\phi^{n+1}) \approx W'(\phi^n) + W''(\phi^n) \times (\phi^{n+1} - \phi^n)$. The resulting equation for ϕ^{n+1} is linear and discretized in space by standard P^1 finite elements. The problem is implemented in AMDiS [24, 25] and the linear system is solved with the direct solver of UMFPAK.

5. Numerical results

We consider 4 examples provided in [19] and take the numerical solutions provided in [19] (with $M = 200$ finite volumes) as benchmark solutions. The problem settings are provided in Table 1.

TABLE 1. Numerical examples, initial parametrization of curve and height profile. $r(l) = 1 + 0.65 \cos(10\pi l)$.

	$\mathbf{X}(0, l), l \in (0, 1)$	h
Problem 1	$\mathbf{X}(0, l) = (\frac{1}{4} + r(l) \cos 2\pi l, -\frac{1}{4} + r(l) \sin 2\pi l)^T$	$h(x, y) = \sqrt{4 - x^2 - y^2}$
Problem 2	$\mathbf{X}(0, l) = (\cos 2\pi l, \frac{1}{10} + \sin 2\pi l)^T$	$h(x, y) = y^2$
Problem 3	$\mathbf{X}(0, l) = (\cos 2\pi l, -\frac{1}{5} + \sin 2\pi l)^T$	$h(x, y) = \sin \pi y$
Problem 4	$\mathbf{X}(0, l) = (\frac{1}{2} \cos 2\pi l, \sin 2\pi l)^T$	$h(x, y) = x^2 - y^4$

Figure 1 shows the zero contour $\phi_\epsilon = 0$ with $\epsilon = 0.025$ of numerical solutions of the degenerate area preserving surface Allen–Cahn equation and the corresponding sharp interface limit as reference solutions for selected time instances. The spatial resolution considers at least 10 mesh points across the projected interface in Ω and the time step is chosen to ensure the CFL (Courant–Friedrichs–Lewy) condition with $\tau \approx k^2$, where k is the corresponding mesh size within the diffuse interface. The mesh is adaptively refined to ensure these conditions. Other numerical parameters are chosen as $\eta = 0.01$ and $c = 2000$. The physical parameters are set as $\beta = 1$ and $\sigma = 1$.

TABLE 2. Hausdorff distance of the planar projections of the curves $\gamma_{200}(t)$ (benchmark solution) and $\gamma_\epsilon(t)$ ($\phi_\epsilon = 0$ level-set) onto Ω in space. Shown are the L^2 -norm in time of the projected Hausdorff distances and the values at the end of the simulation for the four problems shown in Table 1. By then, the equilibrium state has been reached. The last row shows the comparison the same measures for the non-degenerate case with $G(\eta(\phi^n)) = 1$ in the semi-discrete graph-formulation.

ϵ	Problem 1		Problem 2		Problem 3		Problem 4	
	$\ \cdot\ _{L^2}$	equil						
0.1	0.0075	0.0577	0.0014	0.0096	0.0033	0.0211	0.0031	0.0175
0.05	0.0043	0.0332	0.0009	0.0044	0.0019	0.0105	0.0011	0.0069
0.025	0.0032	0.0311	0.0007	0.0026	0.0015	0.0074	0.0007	0.0056
0.025	0.0042	0.0219	0.0039	0.0304	0.0055	0.0094	0.0061	0.0365

We measure the space-time error of the Hausdorff distance for different ϵ of the projected curves $\gamma_{200}(t)$ (benchmark solutions) and $\gamma_\epsilon(t)$ ($\phi_\epsilon = 0$ level-sets) onto Ω . We consider the L^2 -norm in time of this distance. In addition we provide the Hausdorff distance for the reached equilibrium solutions, see Table 2 (first three rows). As the benchmark solution is also just a numerical approximation, we only discuss convergence qualitatively and do not consider any order of convergence. The values at least indicate a reduction of the considered errors. A more detailed and analytically supported convergence study of the numerical solutions requires to extend results of [26] to surfaces, which is beyond the scope of this paper.

In order to demonstrate the importance of the de Gennes factor $1/G(\phi)$ we also consider the four problems without this term. This simply requires to consider

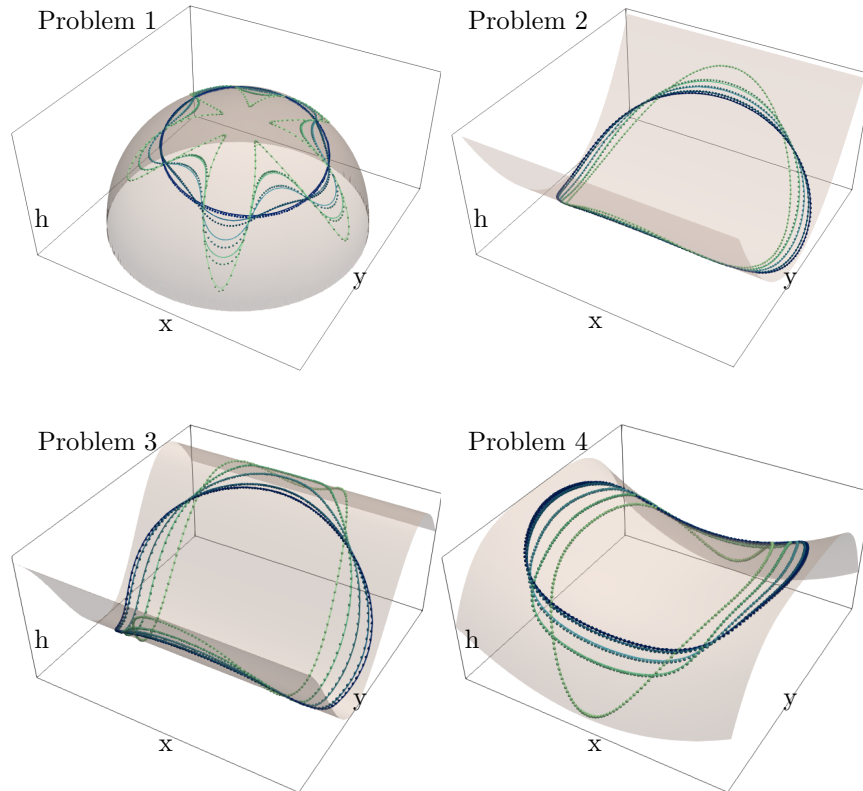


FIGURE 1. Comparison of the numerical solutions of the degenerate area preserving surface Allen–Cahn equation (solid) with the numerical solutions of the corresponding sharp interface limit as reference solutions (dotted). Shown is the zero contour of the phase field function ϕ_ϵ for $\epsilon = 0.025$. The evolution in time is shown in color, running from light green to dark blue. The problem numbers correspond to Table 1 and the time instances shown are *Problem 1*: $t = 0, 0.1, 0.2, 0.4, 1$, *Problem 2*: $t = 0, 0.25, 0.5, 1, 2$, *Problem 3*: $t = 0, 0.5, 1, 2, 4$, and *Problem 4*: $t = 0, 0.25, 0.5, 1, 2.4$.

$G_\eta(\phi^n) = 1$ in the semi-discrete graph-formulation. Figure 2 shows the comparison with the sharp interface solution and the previous results with the de Gennes factor from Figure 1 for $\epsilon = 0.025$ and *Problem 2* as an example. The differences are clearly visible. They are quantified using the same measures in Table 2 (last row) and indicate a significant error reduction. Only for the equilibrium shape in *Problem 1*, which is a circle the error is not reduced. In most cases the error measures for the non-degenerate case are even larger than the corresponding measures for the degenerate case with $\epsilon = 0.1$. The difference certainly depend on the specific geometric setting of the problems. However, the largest differences between the degenerate and non-degenerate problem are found for *Problem 4*, which geometrically is the most complex with both principle curvatures being space-dependent.

Additionally, we analyse the quality of area conservation and the evolution of the system energy (1). The results are shown in Figure 3 and demonstrate the desired properties.

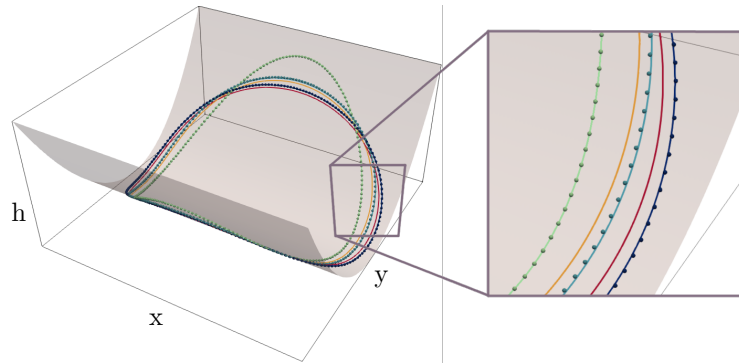


FIGURE 2. Comparison of the non-degenerate and degenerate area preserving surface Allen–Cahn equation (solid) with the numerical solutions of the corresponding sharp interface limit as reference solutions (dotted) for *Problem 2*. Shown is the zero contour of the phase field function ϕ_ϵ for $\epsilon = 0.025$. The evolution in time is shown in color, running from light green to dark blue for the degenerate area-preserving surface Allen–Cahn equation and from light green to dark red for the non-degenerate version. The time instances shown are $t = 0, 0.5, 2$.

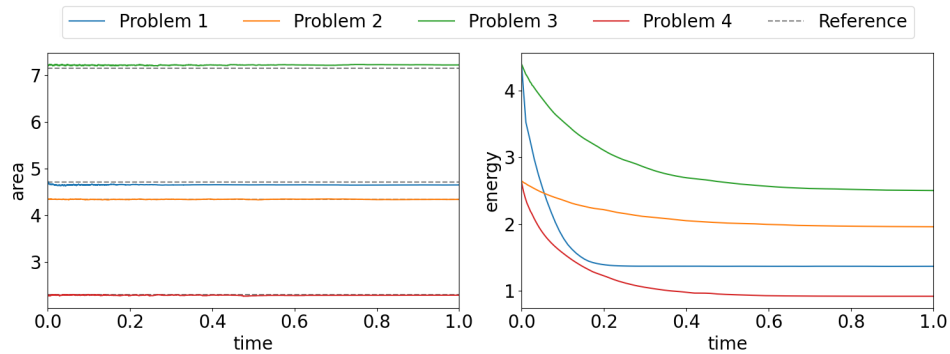


FIGURE 3. Time evolution of the area enclosed by the zero contour of the phase field function ϕ_ϵ (left) and the system energy (1) (right) for $\epsilon = 0.025$. The time is normalized for all four problems. In the left plot we show the reference areas for the four problems according to [19]. For $\epsilon = 0.025$, the maximum absolute deviation from the reference area is 0.082 for *Problem 1*, 0.0180 for *Problem 2*, 0.0745 for *Problem 3*, and 0.0344 for *Problem 4*. The mean absolute deviations are 0.0646 for *Problem 1*, 0.0059 for *Problem 2*, 0.0633 for *Problem 3*, and 0.0133 for *Problem 4*.

We would like to remark that the equilibrium shapes in *Problem 2* and *Problem 3*, which are considered on ruled surfaces, are isotropic. Unrolling the surfaces provides the circular shapes of the final curves. This is consistent with known results for (reaction-)diffusion problems on curved surfaces. E.g. for the surface heat equation it is known that the heat kernel to lowest order only depends on the Gaussian

curvature of the underlying surface [27, 28]. As this is zero for ruled surfaces, the surface should not have any effect on the evolution and a circular equilibrium shape on the surface, as in flat space, can be expected. For the mentioned applications in epithelial tissue, where cells respond to the curvature of the surface, it is essential to resolve these properties.

6. Conclusions

We propose a phase field approximation for area preserving geodesic curvature flow. The considered equation is a degenerate area preserving surface Allen–Cahn equation. The connection between both models is established by formal matched asymptotic analysis and confirmed by numerical solutions for different problems in a graph formulation.

The degeneracy in the surface Allen–Cahn equation results from the de Gennes factor $1/G(\phi)$ in the energy (1), see [13]. While the formal matched asymptotic analysis also holds for $G(\phi) = 1$ the numerical results rely on the de Gennes factor. It ensures $\phi \in [-1, 1]$ much better than without it. This is a desired feature also in 2D and 3D, where the factor $1/G(\phi)$ is used in various applications [15, 16]. However, on curved surfaces it is even more essential as deviations have a more dramatic effect due to the spatially varying geometric properties of the surface which can enhance the resulting errors. These geometric properties also need to be considered in the mesh resolution in the graph formulation. We need to ensure a desired resolution of the projected diffuse interface. Also the additional penalization of the area [23] helps to obtain the shown convergence results. If all these aspects are considered the proposed phase field approximation provides an appropriate way to solve the highly non-linear problem of area preserving geodesic curvature flow by standard tools for solving partial differential equations in 2D and provides the mathematical basis to extend models for epithelial tissue epithelial tissue [8, 9, 10] to surfaces.

Acknowledgments

JMS and AV were supported by the German Research Foundation (DFG) through FOR3013 within project TP05, “Ordering and defects on deformable surfaces” (project number VO 899/30-1). MB and MK were partly supported by the project *21-09093S* of the Czech Science Foundation. We further acknowledge computing resources provided by ZIH at TU Dresden within projects WIR.

References

- [1] P. C. Fife, O. Penrose, Interfacial dynamics for thermodynamically consistent phasefield models with nonconserved order parameter, *Electr. J. Diff. Eq.* 16 (1995) 1–49. doi:10877/7579.
- [2] K. Deckenick, G. Dziuk, C. Elliott, Computation of geometric partial differential equations, *Acta Numer.* 14 (2005) 139 – 232. doi:10.1017/S0962492904000224.
- [3] B. Li, J. Lowengrub, A. Rätz, A. Voigt, Geometric evolution laws for thin crystalline films: Modeling and numerics, *Commun. Comput. Phys.* 6 (2009) 433–482. URL http://global-sci.org/intro/article_detail/cicp/7688.html
- [4] C. M. Elliott, B. Stinner, A surface phase field model for two-phase biological membranes, *SIAM J. Appl. Math.* 70 (2010) 2904–2928. doi:10.1137/090779917.
- [5] H. Garcke, J. Kampmann, A. Rätz, M. Röger, A coupled surface-Cahn-Hilliard bulk-diffusion system modeling lipid raft formation in cell membranes, *Math. Models Meth. Appl. Sci.* 26 (2016) 1149–1189. doi:10.1142/S0218202516500275.
- [6] A. Rätz, A benchmark for the surface Cahn-Hilliard equation, *Appl. Math. Lett.* 56 (2016) 65–71. doi:10.1016/j.aml.2015.12.008.

- [7] C. M. Elliott, L. Hatcher, B. Stinner, On the sharp interface limit of a phase field model for near spherical two phase biomembranes, *Interf. Free Bound.* 24 (2022) 263–286. doi:10.4171/IFB/473.
- [8] B. Palmieri, Y. Bresler, D. Wirtz, M. Grant, Multiple scale model for cell migration in monolayers: Elastic mismatch between cells enhances motility, *Scientific Reports* 5 (2015) 11745. doi:10.1038/srep11745.
- [9] R. Mueller, J. Yeomans, A. Doostmohammadi, Emergence of active nematic behavior in monolayers of isotropic cells, *Phys. Rev. Lett.* 122 (2019) 048004. doi:10.1103/PhysRevLett.122.048004.
- [10] B. Loewe, M. Chiang, D. Marenduzzo, M. Marchetti, Solid-liquid transition of deformable and overlapping active particles, *Phys. Rev. Lett.* 125 (2020) 038003. doi:10.1103/PhysRevLett.125.038003.
- [11] L. Happel, D. Wenzel, A. Voigt, Effects of curvature on epithelial tissue coordinated rotational movement and other spatiotemporal arrangements, *Europ. Phys. Lett. (EPL)* 138 (2022) 67002. doi:10.1209/0295-5075/ac757a.
- [12] L. Happel, A. Voigt, Coordinated motion of epithelial layers on curved surfaces, *Physical Review Letters* 132 (7) (2024) 078401. doi:10.1103/PhysRevLett.132.078401.
- [13] M. Salvalaglio, A. Voigt, S. M. Wise, Doubly degenerate diffuse interface models of surface diffusion, *Math. Meth. Appl. Sci.* 44 (2021) 5385–5405. doi:10.1002/mma.7116.
- [14] S. Dai, J. Renzi, S. M. Wise, Gamma Convergence for the de Gennes-Cahn-Hilliard energy, *arXiv* (2022) 2210.16492. doi:10.1103/PhysRevLett.122.048004.
- [15] M. Naffouti, R. Backofen, M. Salvalaglio, T. Bottein, M. Lodari, A. Voigt, T. David, A. Benkouider, I. Fraj, L. Favre, A. Ronda, I. Berbezier, D. Grosso, M. Abbarchi, M. Bollani, Complex dewetting scenarios of ultrathin silicon films for large-scale nanoarchitectures, *Sci. Adv.* 3 (11) (2017) eaao1472. doi:10.1126/sciadv.aao1472.
- [16] W. B. Andrews, K. L. M. Elder, P. W. Voorhees, K. Thornton, Effect of transport mechanism on the coarsening of bicontinuous structures: A comparison between bulk and surface diffusion, *Phys. Rev. Materials* 4 (2020) 103401. doi:10.1103/PhysRevMaterials.4.103401.
- [17] S. Torabi, J. Lowengrub, A. Voigt, S. Wise, A new phase-field model for strongly anisotropic systems, *Proc. Roy. Soc. A* 465 (2009) 1337–1359. doi:10.1098/rspa.2008.0385.
- [18] A. Rätz, A. Ribalta, A. Voigt, Surface evolution of elastically stressed films under deposition by a diffuse interface model, *J. Comput. Phys.* 214 (2006) 187–208. doi:10.1016/j.jcp.2005.09.013.
- [19] M. Kolář, M. Beneš, D. Ševčovič, Area preserving geodesic curvature driven flow of closed curves and a surface, *Disc. Contin. Dyn. Sys. B* 22 (2017) 3671–3689. doi:10.3934/dcdsb.2017148.
- [20] J. Rubenstein, P. Sternberg, Nonlocal reaction-diffusion equations and nucleation, *IMA J. Appl. Math.* 48 (1992) 249–264. doi:10.1093/imat/48.3.249.
- [21] V. Minárik, M. Beneš, J. Kratochvíl, Simulation of dynamical interaction between dislocations and dipolar loops, *J. Appl. Phys.* 107 (2010) 061802. doi:10.1063/1.3340518.
- [22] M. Beneš, J. Kratochvíl, J. Křišťan, V. Minárik, P. Pauš, A parametric simulation method for discrete dislocation dynamics, *Europ. Phys. J. ST* 177 (2009) 177–191. doi:10.1140/epjst/e2009-01174-7.
- [23] Q. Du, C. Liu, X. Wang, Simulating the deformation of vesicle membranes under elastic bending energy in three dimensions, *J. Comput. Phys.* 212 (2006) 757–777. doi:10.1016/j.jcp.2005.07.020.
- [24] S. Vey, A. Voigt, AMDiS: adaptive multidimensional simulations, *Comput. Vis. Sci.* 10 (2007) 57–67. doi:10.1007/s00791-006-0048-3.
- [25] T. Witkowski, S. Ling, S. Praetorius, A. Voigt, Software concepts and numerical algorithms for a scalable adaptive parallel finite element method, *Adv. Comput. Math.* 41 (2015) 1145–1177. doi:10.1007/s10444-015-9405-4.
- [26] X. Feng, A. Prohl, Numerical analysis of the Allen-Cahn equation and approximation for mean curvature flows, *Num. Math.* 94 (2003) 33–65. doi:10.1007/s00211-002-0413-1.
- [27] J. H. P. McKean, I. M. Singer, Curvature and the eigenvalues of the Laplacian, *J. Diff. Geom.* 1 (1967) 43 – 69. doi:10.4310/jdg/1214427880.
- [28] J. Faraudo, Diffusion equation on curved surfaces. I. Theory and application to biological membranes, *J. Chem. Phys.* 116 (2002) 5831–5841. doi:10.1063/1.1456024.

Department of Mathematics, Faculty of Nuclear Sciences and Physical Engineering, Czech Technical University, 12000 Prague, Czech Republic

E-mail: michal.benes@fjfi.cvut.cz and miroslav.kolar@fjfi.cvut.cz

Institut für Wissenschaftliches Rechnen, Technische Universität Dresden, 01062 Dresden, Germany

E-mail: jan_magnus.sischka@tu-dresden.de and axel.voigt@tu-dresden.de